Botoman (Lower Cambrian) turbid- and clear-water reefs and associated environments from the High Atlas, Morocco

J. JAVIER ÁLVARO[1,2] & SÉBASTIEN CLAUSEN[2]

[1]*Departamento Ciencias de la Tierra, Universidad de Zaragoza, Ciudad Universitaria, 50009-Zaragoza, Spain*

[2]*LP3, UMR 8014 CNRS, Université des Sciences et Technologies de Lille, 59655-Villeneuve d'Ascq, France (e-mail: Jose-Javier.Alvaro@univ-lille1.fr)*

Abstract: Exposures of the Botoman (Lower Cambrian), Lemdad and Issafen formations on the Lemdad syncline, southern High Atlas, provide an excellent example of the interactions between tectonic events, magmatic activity and carbonate productivity. The major factors that controlled the nucleation of carbonate factories on the Botoman High Atlas platform were: (i) synsedimentary tectonism, as normal faulting resulted in tilting of fault blocks causing irregular topographies and subsequent sharp erosion; (ii) volcanism, because pyroclastic influx smothered carbonate factories except in distal areas of the platform or during quiescent episodes of volcanic activity; and (iii) the influence of successive shoaling parasequences. The Botoman reefs exhibit a wide range of external morphologies, including tabular (biostromes) and domal (bioherms and patches) boundstones, which do not exceed 3.5 m of thickness. Although archaeocyathan–microbial reefs only developed under clear-water conditions, microbial reefs grew also under turbid-water conditions. Domal and digitate stromatoids, *Girvanella* crusts, *Epiphyton* bushes and thromboid–stromatoid intergrowths document the ability of some microbial communities to develop heterotrophic strategies when submitted to a moderate terrigenous input. Turbidity was a major ecological factor that constrained development of filter/suspension-feeder and phototrophic organisms, but not necessarily of benthic non-phototrophic microbial communities.

Although it is currently accepted that terrigenous input inhibits carbonate productivity (mainly frame-building factories), new research on modern and Phanerozoic reefs is increasing in siliciclastic shorelines and platforms recording volcanoclastic influence. There, although siliciclastic and volcanoclastic influx affects biotic development, some carbonate factories can exhibit a broad tolerance to continuous or episodic increases in water turbidity (Woolfe & Larcombe 1999; Larcombe *et al*. 2001; Wilson 2000, 2005; Wilson & Lockier 2002). Turbid waters can spread during rifting episodes, as they are associated with distinct volcanic activity, and are commonly accompanied by episodic instability of the sea floor and marked asymmetric changes in sedimentary architecture.

Successive rifting episodes are reported from the Moroccan margin of West Gondwana across latest Neoproterozoic and Cambrian times (Boudda *et al*. 1975, 1979). They are associated with a distinct igneous activity recorded in the Atlas with alkaline and/or tholeiitic affinity (Ezzouhairi 2001). This magmatic activity reflects a tectonic inversion from a Neoproteorozic (Pan-African) compressive margin (Badra *et al*. 1992; Jouhari *et al*. 2001; Ouazzani 2001) to intraplate extension related to latest Neoproteorozic–Early Cambrian rifting processes (Piqué *et al*. 1995).

Hupé (1955) was the first to suggest a major episode of Cambrian reorganization of basinal geometries in Morocco. He tried to explain the apparent occurrence of discordant features associated with the setting of the *Micmacca* Breccia at the base of the Middle Cambrian '*Paradoxides* Shales' in the Anti-Atlas. He associated the setting of this apparent discordance with a supposed 'Salaïrian' tectonic phase in Morocco. Subsequently, Boudda *et al*. (1975, 1979) proposed a widespread subaerial exposure and erosion of large parts of the basin at the end of this episode to explain abrupt modifications in thickness of facies and lithologies. Recently, Álvaro & Clausen (2005, 2006) have related the so-called 'Salaïrian' tectonic phase to a rifting interval with tilting and karstification. Other episodes of basin reorganization predating the Moroccan 'Salaïrian' phase took place in Botoman (Early Cambrian) times, as recorded in the southern rim of the High Atlas. This paper is focused on the analysis of the sedimentary factors that controlled the nucleation, growth and disappearance of the Botoman microbial

From: ÁLVARO, J. J., ARETZ, M., BOULVAIN, F., MUNNECKE, A., VACHARD, D. & VENNIN, E. (eds) 2007. *Palaeozoic Reefs and Bioaccumulations: Climatic and Evolutionary Controls.* Geological Society, London, Special Publications, **275**, 51–70. 0305-8719/07/$15.00 © The Geological Society of London.

and archaeocyathan–microbial reefs that occur in the Lemdad and Issafen formations of the southern High Atlas. This tectonically and magmatically active area of the Moroccan platform favoured development of turbid waters, which directly affected the type of carbonate factories.

Geological setting and stratigraphy

The Neoproterozoic(?)–Cambrian successions of the Moroccan Atlas are located in the Anti-Atlas and central High Atlas mountains, although some disconnected outcrops occur in the Jbilet and Rehamna regions, and the Meseta plateau (Fig. 1a). The axis of the Late Proterozoic–Early Palaeozoic Souss Basin (Geyer 1990*a*) roughly coincides with the modern trend of the Anti-Atlas (SW–NE), where common west-to-east facies changes throughout the Cambrian successions reflect the eastern setting of proximal areas (Destombes *et al*. 1985). To differentiate between the specific palaeogeographical patterns of the High Atlas and the Anti-Atlas, we will refer to them below as the High Atlas and Anti-Atlas platforms.

This paper is focused on the analysis of the Lemdad and Issafen formations cropping out on the Lemdad syncline. The NW-striking Lemdad (from 'Oued el Mdad') syncline, called 'Ouneïn' by some authors, is situated at the southern margin of the west-central High Atlas (Fig. 1b). We have selected for description herewith the westernmost and easternmost outcrops, named sections Le1 and Le11, respectively, by Geyer & Landing (1995). Le1 is the most complete Lower Cambrian section from the High Atlas (Fig. 2): it is the stratotype of the Lemdad Formation (Geyer 1990*a*), and is considered as reference for Lower Cambrian stratigraphic correlations in the High Atlas (see Boudda *et al*. 1975, 1979; Siegert 1986; Geyer & Landing 1995 for lithological and biostratigraphical precisions). Numerous trilobite-bearing strata are known throughout the Lemdad and overlying Issafen formations, which allow identification of the *Antatlasia guttapluviae* and *Sectigena* zones (Geyer 1990*b*) (Fig. 2). In addition, the identification of two major archaeocyathan-bearing reefs in Le1 (previously reported as Ouneïn A and B; see last revision in Debrenne & Debrenne 1995) allows improvement in biostratigraphic correlations. A third archaeocyathan-bearing reef is located in the Lemdad Formation of section Le11; it was previously reported as 'Ouneïn C' or 'bioherme de la cascade' (Fig. 2; see Debrenne & Debrenne 1995 for further information), and is included in the *Sectigena* Zone owing to the presence of the trilobite *Berabichia* cf. *vertummnia* (Heldmaier 1997).

The Lemdad Formation (Geyer 1990a) is a heterolithic succession composed of marlstones, siltstones, limestones and dolostones (some of them microbial and archaeocyathan–microbial reefs), with volcanic ash and volcanoclastic intercalations. It is geographically restricted to a part of the central High Atlas, and its thickness is estimated to be 500 m in the Lemdad syncline. There, a 517 ± 1.5 Ma age is available (Landing *et al*. 1998) from volcanic ashes (sample Le11/10.8 of Geyer & Landing 1995) interbedded in the volcanoclastic sandstones of the Lemdad Formation, and lying in the upper *Antatlasia guttapluviae* Zone of the Moroccan Lower Cambrian Banian Stage (Botoman Stage according to the Siberian scale; Spizharski *et al*. 1986).

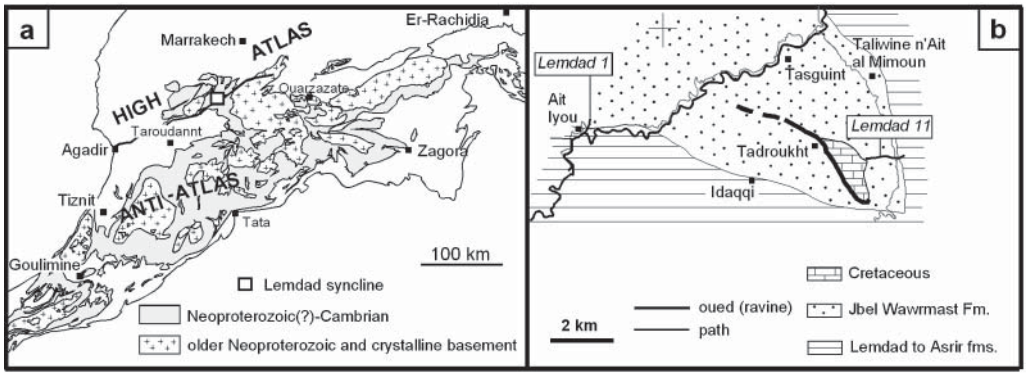

Fig. 1. (**a**) Geological sketch of the Neoproterozoic–Cambrian rocks in the High Atlas and Anti-Atlas, Morocco, with setting of the Lemdad syncline. (**b**) Geological map of the Lemdad syncline with situation of sections Le1 and Le11 (modified from Destombes *et al*. 1985 and Geyer & Landing 1995).

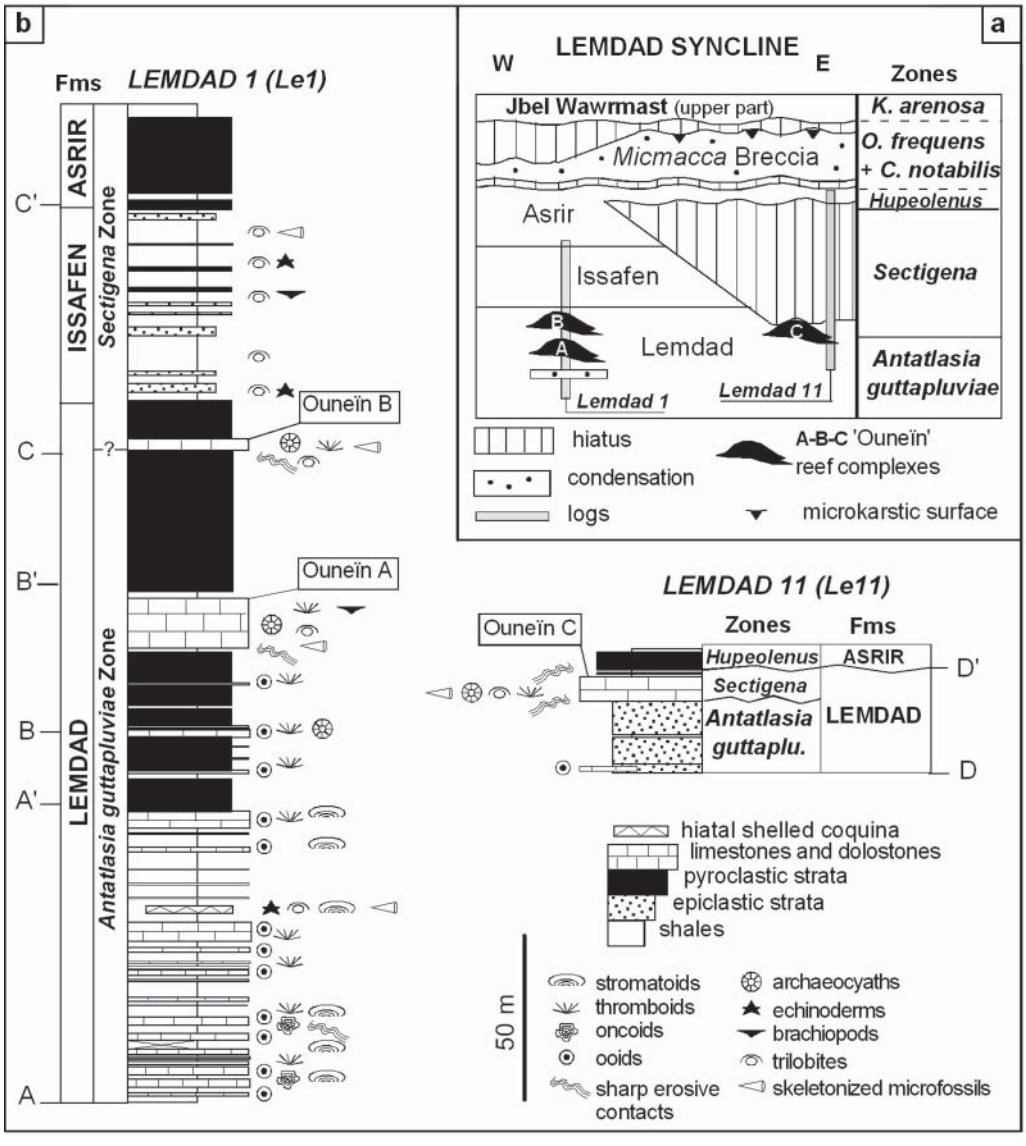

Fig. 2. (**a**) Cambrian stratigraphic framework of the Lower–Middle Cambrian transition in the Lemdad syncline. (**b**) Summarized sections Le1 and Le11 (after Geyer & Landing 1995, Heldmaier 1997 and this work).

The Issafen Formation (26–180 m thick) consists of shales with secondary calcareous and/or sandstone beds in its lower part, and nodular limestones (named 'calcaires scoriacés' by some authors) in its upper part on some areas of the western Anti-Atlas. The formation is widely exposed along the Anti-Atlas and the southern High Atlas. In the Lemdad syncline the formation is extremely thin by erosion. Following the original definitions of 'Série schisto-calcaire' (Choubert 1958), 'Issafene substage' (Boudda *et al*. 1979), Issafen Shales (Siegert 1986) and Issafen Formation (Geyer 1990*b*), the base of the Issafen Formation consists of slightly micaceous, finely laminated shales (Geyer & Landing 1995, p. 20). As a result, we do not place its base at the erosive base of the reef complex 'Ouneïn B', coinciding with a biostratigraphic boundary (as

proposed by Geyer & Landing 1995), but at the occurrence of thick shales overlying the disappearance of volcanoclastic sandstones and conglomerates in Le1. The Issafen Formation shows a drastic decrease in thickness eastwards in the Lemdad syncline, disappearing in Le11 (Fig. 2).

The following sections present description and environmental interpretation of the facies associations found in the Lemdad and Issafen formations of sections Le1 and Le11 (see detailed logs and parasequences in Fig. 3). Facies associations are divided into: (i) volcanoclastic-dominated associations; (ii) carbonate (non-reef) associations; (iii) microbial reefs; and (iv) archaeocyathan–microbial reef complexes.

Volcanoclastic-dominated facies associations

Volcanoclastic sediments are subdivided in this paper into pyroclastic (volcanogenic) and epiclastic strata. The term 'epiclastic' is used to denote sediment where most clasts are derived from weathering of pre-existing sedimentary rocks (Fisher & Smith 1991), despite a minor presence of reworked pyroclasts. In some cases, differentiation of strata primarily composed of reworked pyroclasts and epiclasts can only be made based on matrix composition. For this reason, following Riggs *et al.* (1997), volcanic detritus is referred to as feldspar 'crystals', whereas sediment detritus is referred to as quartz or feldspar 'grains'. In addition, we will follow Smith's (1991) differentiation between: (i) syneruptive sediments, in which the dominant material is pyroclastic, mainly in the ash fraction; and (ii) intereruptive sediments, related to normal or background conditions lacking a significant pyroclastic content both in matrix and clasts.

Tidally influenced epiclastic strata

This facies association occurs exclusively in the Lemdad Formation of Le11, and is made up of amalgamated, large-scale, planar and trough cross-stratified beds. They consist of well-sorted, very-fine to medium-grained arkoses–lithoarenites. The upper and lower boundaries of the individual lenticular sets (0.3–2 m thick) are sharp and some distinctly erosive. They are commonly bounded by millimetre-scale, clay laminae and shaly draps, and display both planar and trough cross-stratification, numerous reactivation surfaces, and parallel, low-angle and wave-ripple lamination. Trough cross-stratification surfaces have a sigmoidal configuration, with tangential bottomset cross-laminae.

The lenticular sets are amalgamated into thickening- and coarsening-upwards sequences, generally less than 4.4 m thick. Palaeocurrents, determined from dip azimuth of foresets (large-scale cross-bedding) and plunge direction of trough axes, demonstrate reverse-flow polarities. Although the dominant flow trends towards the SE (120°–140°), thinner sets capping the thickening-upwards sequences exhibit NNW (290°–330°) palaeocurrents, characterized by less-steep foresets and ripple cross-lamination.

The large-scale, planar and trough cross-stratification, which commonly displays vertical palaeocurrent bimodality, represents part of a system where the dominant current regime changed rapidly from flood to ebb. Although distinct herringbone cross-bedding is absent, the trough cross-stratification shows bi-directional palaeocurrents, dominated by SE (flood) currents, and secondary NW (ebb) ones. Various diagnostic structures document the influence of tidal currents (Meyer *et al.* 1998; Myrow 1998), such as clay laminae (similar to present-day clay drapes occurring in tidal still-stand deposits), reactivation surfaces shown by cross-bedded sets (resulting from time–velocity asymmetry of tidal currents) and bi-directional foreset units. As a result, the reported thickening-upwards sequences may represent progradational trends of bars related to a tidal channel system, in which siliciclastic grains were primarily related to reworking of epiclastic material.

Shoaling epiclastic strata

This facies association occurs in the Lemdad and Issafen formations of Le1. The fine- to medium-grained arkoses and lithoarenites have erosive and abrupt lower and interbedded contacts, scouring into the underlying sediments. It comprises large-scale, trough and planar cross-beddings with sets ranging in thickness from 0.4 to 1.8 m, topped by symmetrical ripples and ripple lamination. Smaller scale sets of trough cross-bedding, of the order of 10–30 cm, are volumetrically less important and occur interbedded with the larger sets. Some intercalated centimetre-thick limestone nodules and layers have yielded trilobite, echinoderm and brachiopod debris, and other undetermined fossils. Palaeocurrent measures from the dip azimuth of foresets of large-scale cross-bedding (thicker than 0.5 m), and plunge directions of trough axes demonstrate unidirectional flow, dominantly north–south, with polymodal foreset migrations ranging from 240° to 330°.

The ubiquity of decimetre-scale cross-bedding indicates that the sandstones were originally deposited as large migrating bedforms. The predominance of trough shapes further shows

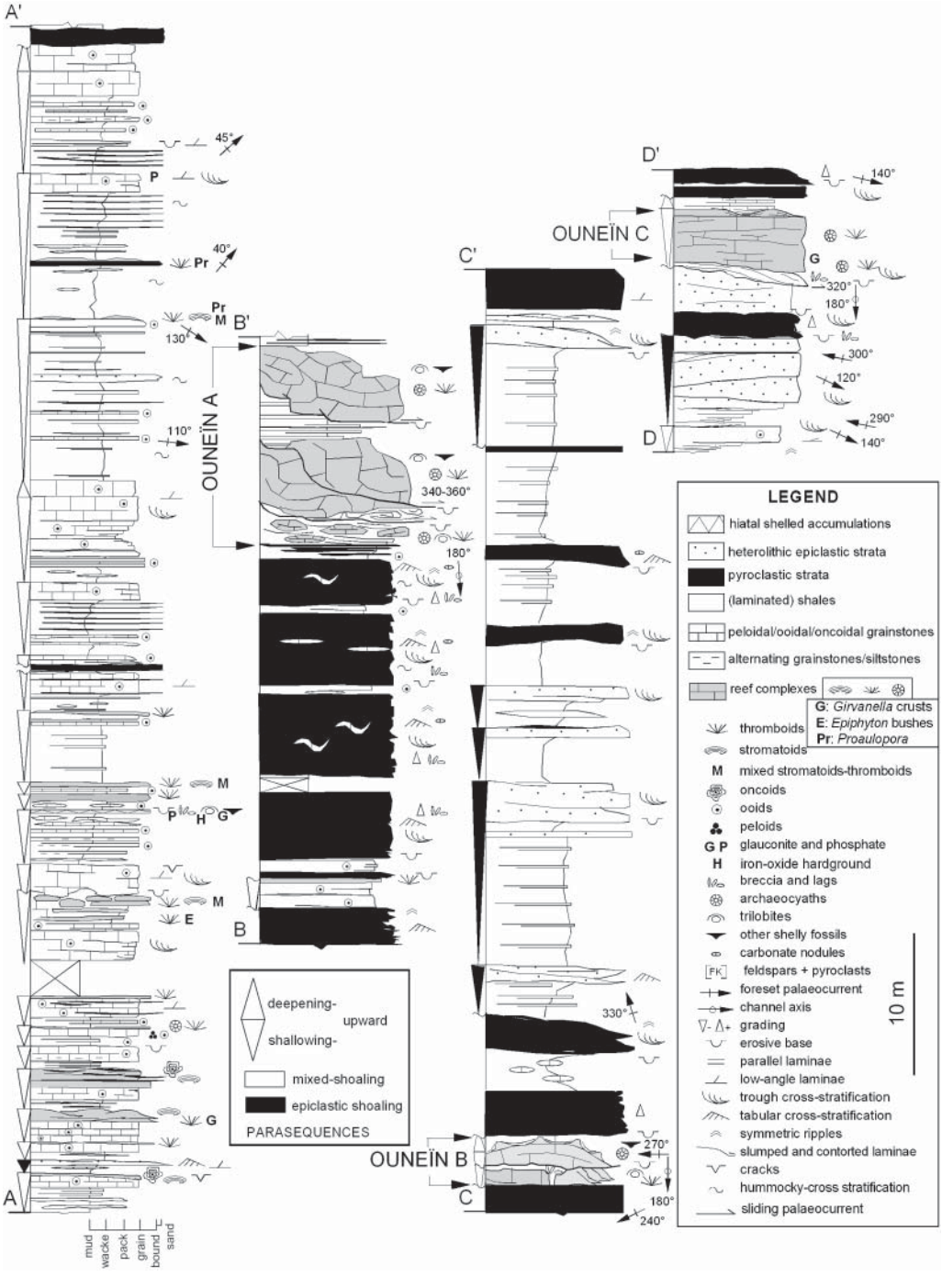

Fig. 3. Representative parasequences of sections Le1 and Le11 (see Fig. 2 for stratigraphic setting of A–A′, B–B′, C–C′ and D–D′).

that they were short-crested megaripples and sandwaves, where reactivation surfaces are rare. The association of sedimentary structures suggests a shallow platform dominated by wave activity, and minor storm reactivation related to interbedded erosive contacts. Episodes in which the bedforms ceased to migrate and were colonized by an open-sea benthic shelled community can be recognized by the presence of marine benthic fossils within carbonate and shale intercalations.

Pyroclastic channels and shoals

Pyroclastic deposits display coarse planar bedding and laminae (Fig. 4a), wave-rippled, and small- to large-scale trough cross-bedding (0.2–1.8 m thick), with lenticular geometries, erosive bases and planar tops (Fig. 4b). Medium-scale cross-laminae, typically dipping subparallel to the imbrication of sigmoidal beds, form the common interval structure of the facies. Channels are filled with thinning- and fining-upwards sets, up to 2 m thick, with a lenticular geometry and erosive bases. Palaeocurrents are similar to those reported in the preceding shoaling epiclastic strata. Pyroclastic strata consist of clast-supported, granule- to medium-grained lithoarenites, with a rounded to very angular, polymictic clast association (Fig. 4c) and an ash matrix. Unstable pyroclastic fragments are composed of microlithic (lathlike), microgranular felsitic or vitric textures, felsitic volcanic rock fragments of feldspar and mafic mineralogy, angular rhyolitic grains, reworked ooidal and bioclastic grainstones and packstones, and hematite clasts. The matrix, less than 10% in volume, consists of silty–sandy rock fragments locally cemented by hematite.

Although pyroclastic dispersal was probably primarily related to sheetwash or hyperconcentrated volcanogenic flow, the pyroclastic material was subsequently reworked by marine wave and benthic currents. The aforementioned sedimentary structures, scarcity of matrix, geometry, grain size and shape suggest that these clast-supported pyroclasts were reworked as marine channels and shoals, induced by wave

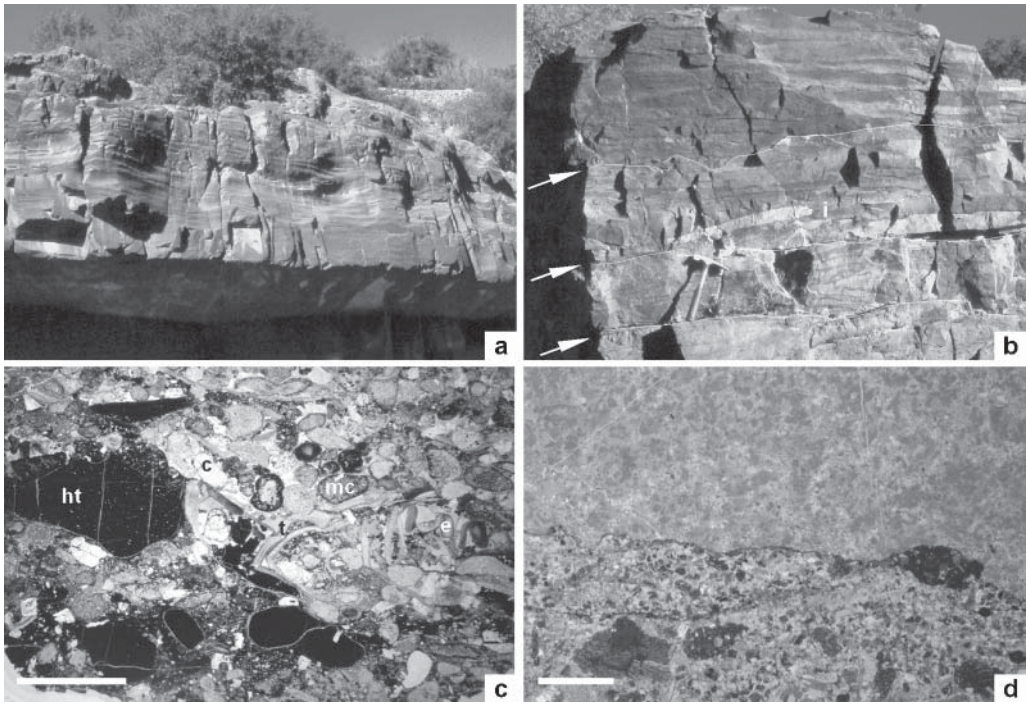

Fig. 4. (**a**) Coarse planar to low-angle bedding and laminae in a pyroclastic sheet. (**b**) Amalgamation of pyroclastic shoals with erosive boundaries (arrowed), covered by lag imbrication (i). (**c**) & (**d**) Thin-section photomicrographs under plane-polarized light. (**c**) Mixed pyroclastic lithoarenite rich in mafic (mc), hematite (ht), polyphase calcite-cemented (c) clasts, and trilobite sclerites (t); scale = 6 mm. (**d**) Pyroclastic lithoarenite (bottom) encrusted by *Epiphyton* bushes (top); scale = 2 mm.

and unidirectional tractions. Locally, the channels and shoals were encrusted by microbial boundstones (Fig. 4d) during episodes of quiescence. The angular feldspars were not significantly transported, but probably yielded by volcanic explosion from neighbouring areas.

Shales and interlaminated claystones and siltstones

These facies underlie, overlie (with onlapping geometries) and are interbedded with the aforementioned shoals, as well as with reef fabrics. They are dominated by fine quartz and angular feldspar silt (the latter locally up to 60% in volume), sericite, illite and muscovite flakes. Shales commonly pass gradually upwards into interlaminated clasystones and siltstones. The former are commonly massive, although their stratification is suggested by the layering of centimetre-thick carbonate nodules, which display bioclastic wackestone textures. Interlaminated claystones and siltstones are laminated at a millimetre scale, and include cross-laminated stringers of silty sand and symmetrical ripples of centimetre scale. Bioturbation, although commonly rare, can locally disrupt bedding. When present, partly articulated skeletons are trilobites, hyolithids and linguliformean brachiopods.

This facies association was deposited on offshore substrates, under calm-water conditions as evidenced by the dominance of siliciclastic mud, and episodic preservation of a partially articulated shelly fauna. The interlaminated siltstones suggest fluctuations in energy, and accumulated above fair-weather wave base.

Carbonate (non-reef) facies associations

Grainstone shoals

They occur as amalgamated beds and lenses, up to 2.4 m thick. They show vertical modifications in composition and texture, changing in ascending order from: (i) intraclastic lags and/or bioclastic packstone–siltstone alternations; to (ii) mixed peloidal–ooidal–pyroclastic grainstones; and (iii) oncoidal-dominated grainstone caps. Microbial reefs (described in next section) encrust some peloidal–ooidal–pyroclastic grainstone foresets and tops, and are also sometimes covered by oncoidal-dominated caps.

(i) The lower, sand- to granule-sized, intraclastic lags (up to 0.1 m thick), which occur overlying scoured bases with flame structures, are clast-supported and chaotically arranged. Clasts are randomly oriented, angular in shape, and commonly consist of packstones of peloids and peloidal aggregates. Lags pass vertically into millimetre-thick peloidal–ooidal packstone–siltstone rhythmites, rich in low-angle erosive surfaces and angular packstone intraclasts (less than 1 cm in size), where the content in siltstone decreases gradually upwards.

(ii) The overlying strata (up to 1 m thick) show undulatory- and planar-laminar bedding, rare low-angle cross-laminae, irregular laminoid fabrics, and numerous low-angle erosive surfaces (up to 3 cm deep). These display gradual transitions between two different textures: peloidal-pyroclastic and ooidal-pyroclastic grainstones. The peloidal-pyroclastic grainstones are composed of 50–70% peloids and peloidal aggregates (up to 1 mm in diameter), 10–30% subangular pyroclasts (up to 4 mm in size), and 5–10% quartz silt. The ooidal-pyroclastic grainstones contain well-preserved ooids (less than 2.5 mm in diameter) with complex radial–concentric cortices. Nuclei are commonly pyroclasts, feldspar and quartz grains, and skeletal fragments. Pyroclasts are very-coarse- to medium-grained sands (less than 2 mm across), subangular–subrounded in shape and some of them polyphasic in nature (Fig. 5a). Scattered bioclasts range from 10 to 40% in volume, and consist of echinoderm ossicles, brachiopod valves and trilobite sclerites. Pyroclasts and feldspars commonly exhibit single or double lamella, a coating process observed too around composite ooids and mixed aggregates of ooids and pyroclasts. The whole framework is cemented with a mosaic of fine, equant–bladed calcite cements (100–300 μm in size) occluding interparticle pores.

(iii) The peloidal–ooidal-pyroclastic grainstones are arranged into thickening-upwards trends (2.0 m thick) capped by microbial reefs (described below) and/or thin (*c.* 0.3 m) oncoidal-dominated grainstone lenses. The size average of the observed rounded–subrounded oncoids is about 1–3 mm (Fig. 5b), although they can reach in some levels 1 cm in diameter. The oncoids commonly show complex cortices evidencing changes in aggregation: for example (i) distinct, wrinkled laminae composed of alternating layers of dense, light-coloured carbonate-rich laminae and porous, darker, organic-rich laminae; and (ii) complex clotted and radial thread-like textures. The nucleus can be a calcite pebble, skeleton or, frequently, an ooid with complex radial–concentric cortices. The whole framework is also cemented with a mosaic of fibrous–equant calcite crystals (less than 300 μm in size). Locally, V-shaped cracks, up to 2 cm deep, developed on the top of the amalgamated grainstones, which

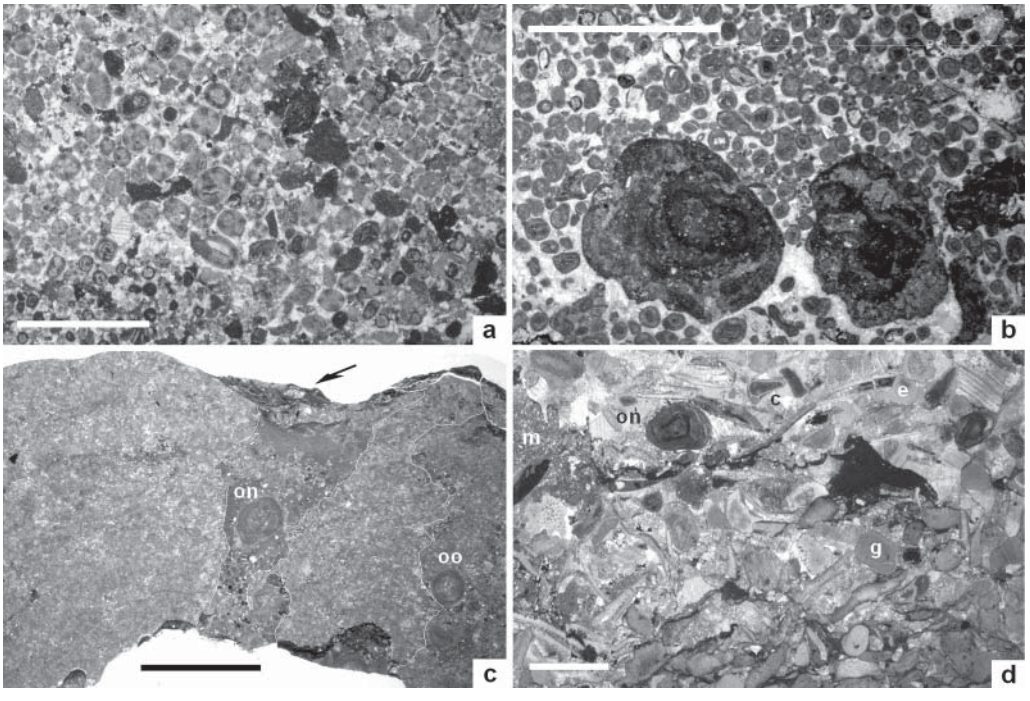

Fig. 5. Thin-section photomicrographs under plane-polarized light. (**a**) Mixed ooidal–pyroclastic grainstone; scale = 1 mm. (**b**) Mixed grainstone with occurrence of larger composite oncoids formed by stromatoid-thromboid intergrowths; scale = 1 cm. (**c**) Silty sparite with V-shaped cracks passively filled with a laminated (arrowed) calcarenite rich in oncoids (on) and ooids (oo); scale = 5 mm. (**d**) Hiatal shelled accumulation with light (parautochthonous) and darker (allochthonous) components, such as glauconite peloids (p), phosphatized oncoids (on), phosphatized chancelloriid sclerites (c), trilobites and echinoderm ossicles, and patches of microsparite (m); scale = 2 mm.

were subsequently passively filled with laminated mixed allochems and skeletons (Fig. 5c).

The intraclastic lags of the amalgamated strata formed by disruption and erosion of coherent rhythmic packstone–siltstone alternations, which were accumulating cemented detritus derived from lateral peloidal and skeletal substrata. The tabular–lenticular shape of the overlying peloidal- and ooidal-pyroclastic grainstones and the preservation of cross-stratified and low-angle laminae suggest deposition as tabular blankets and low- to medium-relief shoals. The sorting, roundness, grading, alternating laminae and basal erosive surfaces of the peloidal–ooidal grainstones suggest intermittent reworking of micritic–peloidal sediments in a medium- to high-energy subtidal environment. The coarsening- and thickening-upwards trends of the amalgamated strata represents deposition in medium-energy, subtidal conditions, shallowing upwards into higher energy, shallow-water inner-platform (likely foreshore) shoal settings, probably as migrating bars and sheets that incorporated extraclasts related to active volcanogenic input. Microbial activity during quiescence episodes of bar migrating is recorded as encrusting microbial reefs (described below), and/or microbial coating of clasts (oncoids). The grainstone sets of Le11 exhibit distinct trough cross-stratification with centimetre-thick sets bounded by shaly laminae and clasts, in which opposite palaeocurrents, probably tidally induced, have been deduced: the thicker and lower parts are ESE-directed, whereas the uppermost thinner parts are WNW-orientated. By contrast, the grainstone sets of Le1 display unidirectional palaeocurrents towards the ESE.

Shelled accumulations

A single bed (30–50 cm thick) is recognized in section Le1 (see top of 11th parasequence in section A–A′ of Fig. 3). It is lined with a lag concentration, less than 5 cm thick, of epiclastic, pyroclastic and limestone debris. The granule clasts are dominantly angular, whereas the sand-sized

clasts are subangular–subrounded in shape. The lag changes upwards into packstone–breccia textures, the latter rich in pyroclastic granules, locally displaying low-angle laminae. They contain sand-sized glauconitic peloids, and disarticulated to broken echinoderm ossicles and trilobite debris, and secondary sponge spicules, chancelloriid sclerites, brachiopods and helcionellids. Both litho- and bioclasts can be subdivided into primary (without epigenetic replacements) and reworked (polyphase) clasts (Fig. 5d). The allochthonous clasts contain cores of first-generation granules and skeletons with accretionary sediment. Hematite and phosphate typically occur as thin coatings or impregnations around and within selective debris, and also stain mineral (feldspar) and skeletal heterogeneities. Matrix varies from a mixture of calcite micrite and microsparite, detrital dolomite and terrigenous silt and sand in variable proportions. Micrite occurs in scattered pockets and lenses (up to 1 cm long), sometimes filling intraparticular primary geopetal structures discordant with shelter fillings and stratification. Spar-filled voids have irregular walls and a primary skeletal support. Primary shelter pores commonly formed beneath elongated trilobite sclerites and brachiopod valves. Bioturbation is absent.

The polyphase character of some clasts suggests multiple depositional, cementation and erosive events. The shelled accumulation is interpreted as derived from washing and reworking of skeletons and other allochems from the surrounding sea floor generating low-angle shoals under high-energy conditions. The presence of a selective diagenetic precipitation of iron oxides and phosphate allows differentiation in parautochthonous (unaffected) and allochthonous (secondarily reworked after hematite and/or phosphate epigenesis) skeletons, because polyphase litho- and bioclasts are selectively coated or replaced by hematite and phosphate, a cement that generally occluded the primary (intraparticular) porosity. This facies association has been previously described in the overlying *Micmacca* Breccia, described and interpreted by Álvaro & Clausen (2005, 2006) as composite event-concentration, low-relief shoal complexes composed of parautochthonous and allochthonous skeletal assemblages representing hiatal shelled accumulations (*sensu* Kidwell & Bosence 1991).

Microbial reefs

The term 'reef' is used here because the framebuilding fabrics are dominated by peloidal, thromboid and stromatoid textures, rather than homogeneous mud fabrics. The fabrics correspond to 'Frame Reefs' (*sensu* Riding 2002), in which in-place skeletons (including calcified microbes) are in contact and microbial clotted-peloidal fabrics are considered as microframe structures.

Stromatoid crusts

They show crinkled, bulbous, domal (up to 1 cm in diameter and 4 cm high), and digitate columnar morphologies embedded in a silty microsparite. Stromatoids consist of alternating layers of dense, light-coloured carbonate-rich laminae, extremely rich (up to 60% in volume) in silty, quartz, mica and feldspar crystals and grains, and darker, organic-rich laminae with pyroclastic material less than 10% in volume (Fig. 6a). Interdomal areas are either filled with fine-grained bioclastic wackestones (with trilobite sclerites and skeletonized microfossiles), rich in silty quartz and feldspar grains and crystals, or host smaller domal and crinkled stromatolites that are gradually enveloped by the larger accreting domes. These stromatoids represent accretion of microbial mats and biofilms developed under turbid waters, and fit with Riding's (1991) concept of 'agglutinated stromatolites'.

Girvanella *crusts*

This calcimicrobe shows a variable preservation, from well-defined filaments to threads of micrite. It occurs as sheets and crusts of intertwined filaments (Fig. 6b), generally horizontal but also inclined at low to high angles with the stratification plane. Dispersed *Girvanella* bundles form biodictyon structures (*sensu* Krumbein *et al.* 2003) embedded in a micritic matrix where distribution of silty quartz and/or feldspar grains/crystals is highly variable, ranging from 5 to 40% in volume. These microbial sheets and biofilms encrusted and stabilized soft carbonate muddy–silty substrates. Pyroclastic influence, when present, did not affect their development.

Epiphyton *bushes*

Epiphyton is the most prolific calcimicrobe and form dense masses of grey clumps (Fig. 4d). Its shrubs commonly branch and bifurcate upwards and sideways, reaching up to 10 cm in thickness. The boundstones are massive, and composed of irregular layers of *Epiphyton*, although *Renalcis* clots are locally present, but secondary in volume. This boundstone is embedded in a siltstone that changes laterally into a silty sparry cement, composed of fibrous and bladed calcite

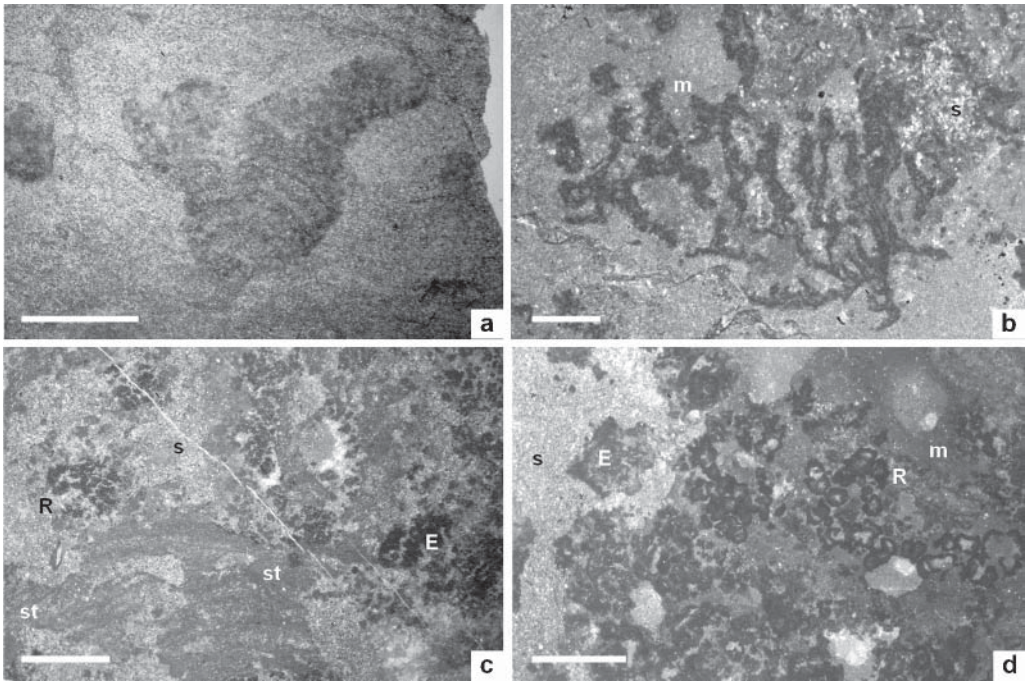

Fig. 6. Thin-section photomicrographs under plane-polarized light. (**a**) Agglutinated stromatoid digitate columns rich in silt trapped and bound by the former microbial communities; scale = 5 mm. (**b**) *Girvanella* filaments and threads reflecting episodic encrusting of a variable substrate, ranging from carbonate muddy (m) to silty granular (s); top on the right; scale = 1 mm. (**c**) Thromboid–stromatoid intergrowth where successive agglutinated stromatoid generations (st) are differentiated by their onlapping geometries, encrusted by several *Epiphyton* (E) and *Renalcis* (R) bushes, the whole framework embedded in a silty (s) matrix; scale = 4 mm. (**d**) Replacement of *Epiphyton* (E) to *Renalcis* (R) bushes related to a sharp contact from silty (s) to muddy (m) substrate; top on the right; scale = 3 mm.

cements (100–300 μm across). The siltstone component, locally up to 40% in volume, consists of slightly abraded, euhedral feldspar crystals, euhedral and reworked quartz crystals and grains, and minor disarticulated fossil debris (mainly trilobite sclerites). The siltstone not only occurs dispersed in the grainstone embedding the microbial boundstone, but is also covered by boundstone textures forming both silty patches within the microbial boundstone and boundstone patches embedded in a silty matrix. This evidences growth of frame-building textures related to turbid waters.

Thromboid–stromatoid intergrowths

These microbial reefs are a complex intergrowth of thromboids, with *Epiphyton* as dominant calcimicrobe (up to 40% in volume), and local development of crinkled and domal stromatoids (Fig. 6c). The whole framework forms irregular crusts, changing laterally from 0 to 20 cm in thickness, which covers the top of some of the aforementioned grainstone shoals, as well as some of their foresets. Archaeocyathan debris is extremely rare or absent. The microbial framework is composed of subunits bounded by erosive discontinuities. Each subunit changes vertically from an intraformational lag, rich in reworked microbial clasts embedded in a peloidal–microbial packstone, to a complex crust, composed of an intergrowth of *Epiphyton*, *Girvanella*, *Renalcis* and rarer domal stromatoids, preserved in growth position (Fig. 6d). Growth cavities between the thromboid–stromatoid consortium have calcarenitic infillings and are encrusted by fibrous to bladed, calcite cement (100–300 μm in size). Internal sediment consists of a silty sparitic calcarenite rich in feldspar crystals (reaching locally 50% in volume), quartz and mica grains, minor disarticulated skeletal debris (rich in micritized, trilobite sclerites and echinoderm ossicles), and reworked (intraformational) microbial debris.

These fabrics developed as centimetre-scale bushes or clumps above the surrounding sea floor forming a depositional relief with ongoing physical deposition of sediment between the locally digitate boundstones. The cap of the frame-building subunits commonly consists of microbial packstones, dominated by *Proaulopora* tubes (commonly fragmented), peloids, intraformational lumps and silty feldspar crystals. *Proaulopora* filaments, 40–130 μm in diameter and up to 500 μm in length, are straight to slightly curved tubes, sometimes bifurcated in longitudinal section. The possible binding role of *Proaulopora* was constrained by high-energy conditions, and the lack of self-supported structures and microbial biofilms able to stabilize the sediment. In summary, these thromboid–stromatoid intergrowths episodically recorded the influence of high-energy benthic currents, which reworked part of the microbial framework and formed the described subunits bounded by erosive discontinuities. This microbial consortium commonly grew under turbid waters as evidenced by the wealth of embedded pyroclastic and epiclastic material.

Archaeocyathan–microbial reef complexes

Three reef complexes have been identified: Ouneïn A, B and C (the latter also named 'bioherme de la cascade'; Fig. 3). The systematics of the archaeocyaths was updated in Debrenne & Debrenne (1995), whereas their trilobites and skeletonized microfauna were reported in Geyer & Landing (1995).

As core textures are similar in the three reef complexes described below, they are described in this section in order to avoid repetitions. The boundstone consists of a complex intergrowth of *Girvanella*, *Epiphyton* and *Renalcis*, with variable numbers of archaeocyaths, rarely exceeding 20% in volume. Some of the archaeocyaths are attached as outgrowths fixed on other archaeocyathan walls (Fig. 7a), the whole framework encrusted by luxuriant *Epiphyton* and *Renalcis* overgrowths. Dweller organisms were trilobites, echinoderms, calcite- and phosphate-shelled brachiopods, hyoliths, chancelloriids and other skeletonized microfossils. Burrowing is nearly absent. Growth cavities between this framework are lined by fibrous–bladed calcite (100–300 μm across), and lack significant percentage of silty component (different from the flanks, described below, where it is abundant; Fig. 7b, c). Internal sediment is generally a microbioclastic wackestone with scattered microbial fragments. Three distinct matrix textures are preserved: peloidal, clotted and homogeneous, which can interchange both vertically and laterally. Peloidal textures consist of irregular silt- to sand-sized peloids of microcrystalline calcite embedded in a groundmass of calcite microspar and pseudospar. Peloidal matrix grades into clotted micrite. Finally, homogeneous micrite occurs as millimetre-thick lenses and discontinuous laminae. Reef soles (underlying the reef cores), up to 10 cm thick, consist of irregular skeletal–peloidal wackestones and packstones, which directly overlie the pyroclastic strata and breccia beds that acted as nucleation surfaces for reef growth. By contrast, reef covers, up to 20 cm thick, commonly contain silty packstones rich in microbial and shelled accumulations composed of *Proaulopora* filaments, trilobites, hyoliths and other microfossils, similar to the aforementioned cover of the thromboid–stromatoid intergrowths.

'Ouneïn A'

The archaeocyathan–microbial reef complex occurs in a lateral ravine of the Lemdad oued (Fig. 7e). Three geometries are identified vertically. The lower part consists of archaeocyathan–microbial patches, recognized as isolated pillow-shaped masses, ranging in size from 0.2 to 2 m and from 0.2 to 1 m high, underlain, surrounded and onlapped by the aforementioned pyroclastic shoals and laminated shales. This volcanosedimentary unit, up to 1.6 m thick, is directly covered (in the lateral ravine) by a tabular archaeocyathan–microbial reef, up to 2.6 m thick, dominated by archaeocyathan-rich floatstone textures, although some decimetre-thick boundstone lenses can be recognized towards the top. The biostrome exhibits numerous fractures dipping nearly vertically, and striking E–W. Finally, two lobated megabreccia accumulations occur along the ravine, up to 5.2 m thick, which are in contact with a synsedimentary fault (Fig. 7e). They are characterized by metre-sized olistoliths, and a mixture of angular fragments, granule–boulder in size (up to 2 m in diameter). These have chaotic orientations and boundstone to floatstone textures. The clasts are embedded in a matrix composed of thinly bedded and contorted shales, laminated marlstones, calcareous or silty claystone and deformed claystone clasts, and pyroclastic debris lying the boulders.

Both megabreccia bodies represent redeposited fragments of the eastern neighbouring reef biostrome. These accumulations along the margin of a synsedimentary fault are not related to reef collapse by overbuilding owing to the thin relief of the source reef, and the presence of

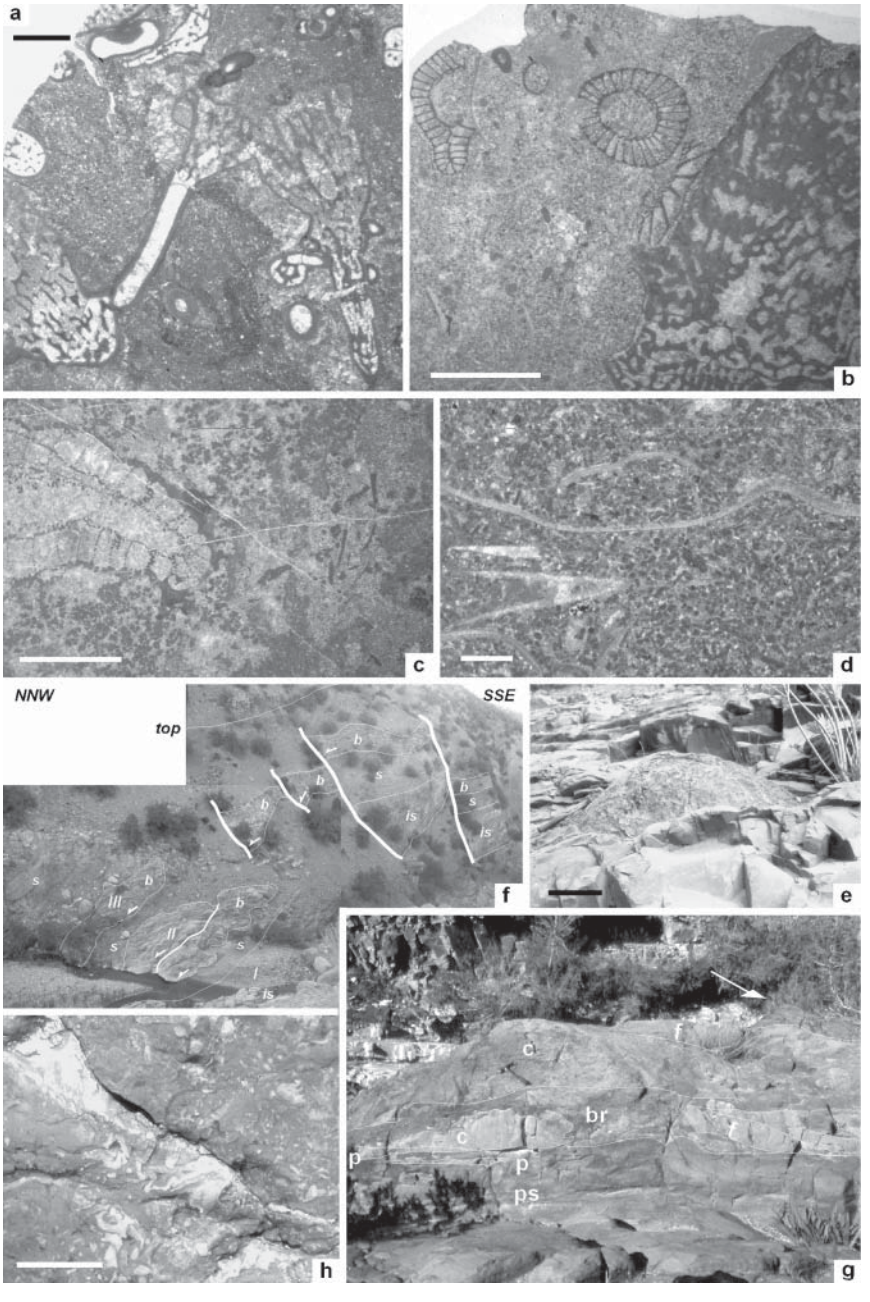

Fig. 7. (**a**) Archaeocyathan–microbial boundstone from Ouneïn B with longitudinal sections of encrusting archaeocyathan cups; scale = 2 mm. (**b**) Archaeocyathan floatstone rich in siltite matrix from Ouneïn B; scale = 5 mm. (**c**) Contact between archaeocyathan–microbial boundstone (left) and flank composed of siltite floatstone (right); scale = 5 mm. (**d**) Reef cover composed of a packstone rich in *Proaulopora*, and trilobite and hyolithid debris; scale = 1 mm. (**e**) Patch reef capping the reef complex Ouneïn B; scale = 10 cm. (**f**) Field aspect of Ouneïn A: b, breccia; s, shales with interbedded ashes and pyroclastic lithoarenites; is, *in situ* reef patches and biostromes; I–II–II, three breccia lobes; arrows, sliding palaeocurrents; 'top' marks the burial of the synsedimentary palaeotopography by pyroclastic strata. (**g**) Geometry of the bioherms of Ouneïn B finally capped by patch reefs (arrowed): ps, pyroclastic shoal; p, packstone sole; br, breccia; c, core; f, flank. (**h**) Breccia underlying Ouneïn C rich in carbonate and skeletal clasts; scale = 5 cm.

pyroclastic tuffs and ashes interbedded with the lobes and reworked within them, which reflect perturbations related to volcanic activity.

'Ouneïn B'

This reef complex can be subdivided into four stratigraphic levels (Fig. 7g), in ascending order: (i) a lower bioherm displaying distinct core and flanks; (ii) an irregular breccia; and (iii) a second bioherm where flanks are not well preserved, finally capped by (iv) numerous patch reefs (Fig. 7f), subsequently onlapped by laminated shales.

Both bioherms (i and iii), which display a marked tendency for aggregation, are less than 1.5 m thick and can be followed laterally up to 4 m. The flanks of the lower bioherm are generally thinly bedded (0.1–0.3 m), limestones with floatstone textures that show primary depositional slopes dipping up to 40°. They thin away from the core, passing laterally, over a distance of 2 m, into debris beds. Debris textures and grain size are highly variable with larger, centimetre-sized clasts of boundstone textures common in proximal positions. The clasts are chaotically arranged and commonly set in a matrix of bioclastic wackestone or poorly sorted packstone. Some core-facies material is reworked into the proximal flank sediments. Scours within the cores attest to episodic erosion of the surface, responsible for yielding the clasts present in the debris beds. In some cases *in situ* calcimicrobes grew as small bushes or clumps above the surrounding archaeocyathan–microbial floatstone.

The lower bioherm is topped with a distinct erosive channel (Fig. 7g). This is filled with a thin (less than 1.4 m), clast-supported breccia (rich in pyroclasts and boundstone–floatstone clasts up to 2 cm across), with intrabreccia erosive surfaces lined with centimetre-thick siltstone layers. The bottom of the channel cuts down into the bioclastic sole of the lower bioherm exposing its volcanoclastic substrate.

The upper bioherm, up to 1.6 m thick and 3 wide, is only recognized by its core. Its margin is not exposed in outcrop, so the nature of flanking strata is unknown. It is directly covered with numerous patch reefs (less than 0.8 m in diameter and height; Fig. 7e). The onlapping geometries of the overlying shales indicate that the patches were indeed topographic irregularities on the sea floor.

'Ouneïn C'

The two-dimensional exposure of the reef complex prevents determination of its broad shape. Anyway, as a whole, the reef complex shows three stratigraphic levels, from bottom to top: (i) a lower breccia body (up to 40 cm thick; Fig. 7h) related to a distinct underlying erosive surface; (ii) a stratiform frame-building body, up to 3.4 m thick; and (iii) a series of laterally related patch reefs, with flat bottom and convex tops, up to 0.5 m thick and 1.4 m in diameter.

The reef complex in underlain by a sharp erosive surface, planar–deeply scoured, which exhibits sharp changes of its steeped slopes that make angles up to 80º with the horizontal stratification. The surface is clearly demarcated truncating the underlying tidally influenced epiclastic strata, passing northwards to oblique and paralleling the overlying carbonate strata. The overlying breccia displays a coarse trough cross-bedded stratification with foreset migration towards the NNW. Both the erosive surface and the overlying cross-bedded breccia show NNW orientations, so that, according to the palaeogeographical models of the Souss Basin (Destombes *et al.* 1985; Geyer & Landing 1995), the brittle fracturation that induced the discontinuity was sloping landwards. There is a variety of clast sizes and types, some of them polyphase in character, such as angular–subrounded pyroclasts (e.g. mafic and rhyolitic clasts less than 6 cm across, although most clasts do not reach 2 cm in diameter), cemented by a sparry calcite (*c.* 0.2 mm across), locally dolomitized. Angular feldspars are common, whereas fossils skeletons (such as micritized archaeocyaths, echinoderm ossicles and other microfossils of uncertain affinity) and breccia composed of boundstone and floatstone clasts (up to 4 cm across) are locally abundant (Fig. 7h). Carbonate and skeletal clasts are typically angular–subangular in shape, poorly to very poorly sorted, and were secondarily dolomitized, silicified or simply recrystallized.

The middle part of the reef complex, overlying the aforementioned breccia, consists of a distinct glauconitic marker bed, up to 0.5 m thick. The marker bed is texturally a siltstone that contains glauconitic peloids (up to 2 mm in diameter and 70% in volume), and secondary pyroclastic fragments (up to 6 mm across), fossil debris, mostly trilobites, and siliciclastic grains (less than 0.6 mm across) of subangular feldspars, quartz and mica. The whole framework is locally cemented by sparry calcite. Glauconites occur as subrounded and medium-sorted peloids, in some cases somewhat fragmented and reworked. Although the original stratification is not well preserved, the fact that the glauconitic peloids commonly have their long axes at low angles to bedding seems to rule out compaction as the

main mechanism to explain their grain orientation. This marker bed displays an upwards increase of micrite, associated with a fall in pyroclastic material, leading to the nucleation of an archaeocyathan–microbial biostrome. Archaeocyaths increase in abundance upwards and become the major constituent at the top. Frame-builder skeletons are commonly micritized, preserved upright, although secondarily parallel to bedding, and their primary intraparticular porosity locally occluded by bladed sparite (100–200 μm in size).

The upwards decrease in pyro- and epiclasts and glauconitic peloids is replaced by an increase in microbial and archaeocyathan debris, whose erect preservation (boundstone) becomes dominant towards the top. The top of this apparent biostrome is covered with metre-scale patch reefs. The whole reef complex is onlapped by millimetre- to centimetre-thick alternations of siltstones and bioclastic packstones. The latter are rich in trilobites covering sparry shelter structures. The terrigenous fraction comprises angular feldspars, pyroclasts and micas, petrographically assigned to an arkosic and lithoarenitic greywacke.

The unoriented, unsorted and poorly rounded to angular clasts, and the lack of both bioturbation and lime-mud in the lowermost breccia body, suggests the possibility of mixing by mass flow along a palaeoslope. Intraclasts were directly derived from erosion of the lateral continuity of either this reef complex or from other ones. The clast-supported breccia is interpreted as debrites deposited by viscous mass flows, often with a lenticular geometry indicating that the breccia unit had an original relief above the sea floor. The breccia deposited likely as a result of reworking by traction processes of local lag deposition from bypassing high-concentration gravity flows. Owing to the lack of grading arrangements, it should be better interpreted as scars or gullies in a slope, rather than channels filled by tectonically induced deposits generated by different types of flow. There are no morphological criteria to interpret it as a submarine fan, but as an episodically reworked palaeoslope that acted as its own source of sediments.

Glauconites formed as sea floor peloids. Their deep emerald green colour corresponds to mature, highly evolved, K_2O-rich glauconite mica (Odin & Fullagar 1988; Amorosi 1995). These authigenic minerals are interpreted as deposited in open-marine environments with very slow deposition rates, once the breccia-deposition events ended. The glauconitic peloids probably formed as a result of dissolution–precipitation processes (described by Chafetz & Reid 2000), and were reworked short distances although not derived by erosion of older rocks.

The gradual decrease in sand content upwards and the increase in micrite favoured nucleation of an archaeocyathan–microbial biostrome, although its morphology is based on reduced outcrop exposure and its whole dimensions are unknown. The influence of volcanic activity is irregularly recorded across the whole reef complex as silty feldspar, quartz and pyroclasts. This environment ended sharply, and the frame builders developed metre-thick patch reefs. Their flanks recorded high-energy alternations of packstones and siltstones reflecting a progressive deepening-upwards trend accompanied by shale onlapping, which was sharply interrupted by the input of coarse-grained pyroclasts.

Parasequence framework

The southern High Atlas platform recorded across Botoman times a mixed (carbonate–epiclastic) sedimentation, characterized by stacked, small-scale, shallowing-upwards trends (parasequences *sensu* Van Wagoner *et al.* 1988). These were episodically interrupted by tectonic perturbations and the input of large amounts of pyroclastic material (see Fig. 3), which directly affected the patchy occurrence of microbial and shelled carbonate factories. Correlation of small-scale parasequences across the Lemdad syncline is difficult owing to the development both of stratigraphic gaps related to erosion (e.g. the whole Issafen Formation in section Le11; Fig. 2) and hiatal shelled accumulations, drastic lateral changes in thickness of pyroclastic material according to the distance to magmatic sources, the seawards dissapearance of the tidal influence (dominant in Le1 but absent in Le11), episodes of local tectonic tilting and subsequent lateral changes in erosive depths, and the discontinuous distribution of carbonate productivity. Syn-sedimentary structural control during deposition of the Lemdad Formation is evidenced by abrupt, lateral and vertical changes in carbonate facies (reflecting differential subsidence of fault-bounded blocks) and thickness, and widespread development of slope-related facies associations rich in conglomerates, breccia lobes, erosive cicatrices, and slumping and sliding structures (see Fig. 3). Tectonically induced subsidence with concomitant base-level change (related to emplacement and reworking of volcanic flows: Smith 1991) probably created accommodation space farther than it could be filled by pyroclastic input inducing syneruptive aggradation of pyroclastic material.

Although the input of allochthonous pyroclastic material cannot be related to distinct parasequences, the Botoman mixed (carbonate–epiclastic) facies associations of the Lemdad syncline are arranged into two kinds of shallowing-upwards parasequences: mixed and epiclastic shoaling parasequences (Fig. 3). The bases of the parasequences are flooding surfaces, whereas their tops are bounded by erosive discontinuities that have undergone substantial channelling and/or slumping, and are directly overlain by reworked intraclasts.

The Botoman platform of the Lemdad syncline recorded an evolution from carbonate- to epiclastic-dominated sediments, punctuated by a major episode of pyroclastic blanketing related to magmatic activity in neighbouring areas. This evolution is more complete in the distal part of the studied outcrops (Le11) because the proximal ones (Le1) contain an erosive hiatus that erased the sedimentary record of a part of the Lemdad Formation and the whole Issafen Formation. In Le1, the parasequences of the Lemdad Formation display a distinct tidal influence, which is absent in Le11. The older (stratigraphically lower) part of the distal Lemdad Formation (section A–A′ of Le1; Fig. 3) is characterized by the vertical superposition of mixed shoaling parasequences. These, 1.2–10 m thick, are composed, from bottom to top, of: (i) offshore shales and bioclastic wackestones; (ii) millimetre-thick grainstone–siltstone alternations; and (iii) prograding ooidal–peloidal-pyroclastic grainstone shoals that record high-energy water conditions above fair-weather wave base. Some parasequences also pass vertically into (iv) microbial boundstones, and/or (v) oncoidal grainstones, partly dolomitized and covered by ferruginous crusts and reworked intraclasts. The tops of the parasequences are bounded by minor discontinuities, easily recognized by the development of microbial crusts, erosive surfaces, V-shaped cracks, dolomitized beds and reworked intraclasts. As a result, the parasequences are interpreted to have formed as prograding carbonate shoals on an open-marine platform (suggesting deposition by storms and waves from upper shoreface to foreshore) that reworked ooids, peloids, oncoids, aggregates, intraclasts and fossils. The setting of microbialites encrusting the foresets of grainstone shoals indicates episodes in which the shoal bedforms ceased to migrate and were locally stabilized by microbial biofilms and crusts. However, the aforementioned stromatoid crusts, *Epiphyton* bushes and thromboid–stromatoid intergrowths mainly nucleated: (i) on protected (back-shoal) settings; and (ii) upon the topographic highs yielded by the foreset shoals during episodes of quiescence. In both cases, they developed under turbid waters. *Proaulopora* debris capped some microbial reefs forming microbial bioaccumulations in high-energy environments.

Subsequently, a major episode of pyroclastic input dramatically affected this platform (section A′–C of Le1; Fig. 2). The aforementioned mixed shoaling parasequences developed incompletely among the pyroclastic pulses, which were associated with tectonic instability of the platform. These perturbations are linked with nucleation and growth of the metre-sized archaeocyathan–microbial reef complexes of the area. The latter (i) occur sandwiched between pyroclastic blanketing pulses, (ii) are related to tectonic events and erosive surfaces, and (iii) disappeared by flooding and shale onlapping. The second point is documented by the breccia lobes associated with the tectonically induced footwall highs that laterally bound the partially preserved biostrome of Ouneïn A, the breccia that underlies the upper bioherm of Ouneïn B (the lower one grew directly on a pyroclastic substrate), and the breccia that underlies the biostrome of Ouneïn C.

A flooding of the platform is recorded across the Lemdad–Issafen transition, characterized by a fall in pyroclastic blanketing, and the establishment of epiclastic shoaling parasequences in an offshore-dominated platform. The succeeding epiclastic shoaling parasequences consist of coarsening- and thickening-upwards sequences, 1–12 m thick. From bottom to top, almost all the sequences display a systematic succession in which finer-grained storm deposits are covered gradationally or sharply by coarser-grained, cross-stratified sandstones. The top of some parasequences display erosive and truncating surfaces, partly stained by ferruginized hardgrounds, and locally highly bioturbated by *Skolithos* and *Arenicolites*. Shoaling (prograding trends related to shallowing-upwards fluctuations of the relative sea level) during times of rapid sediment influx offers a simple and repeatable mechanism for creating these coarsening-upwards sequences, topped by hardgrounds widely bioturbated.

Palaeogeographical setting and turbidity

Synsedimentary tectonism across the Botoman is manifest in the Lemdad syncline, and deeply influenced regional bathymetric changes and local submarine topography. The Lemdad reefs developed on the southern High Atlas platform did not accumulate on an intact, uniformly subsiding segment of the High Atlas platform, but instead on a mosaic of differentially subsiding,

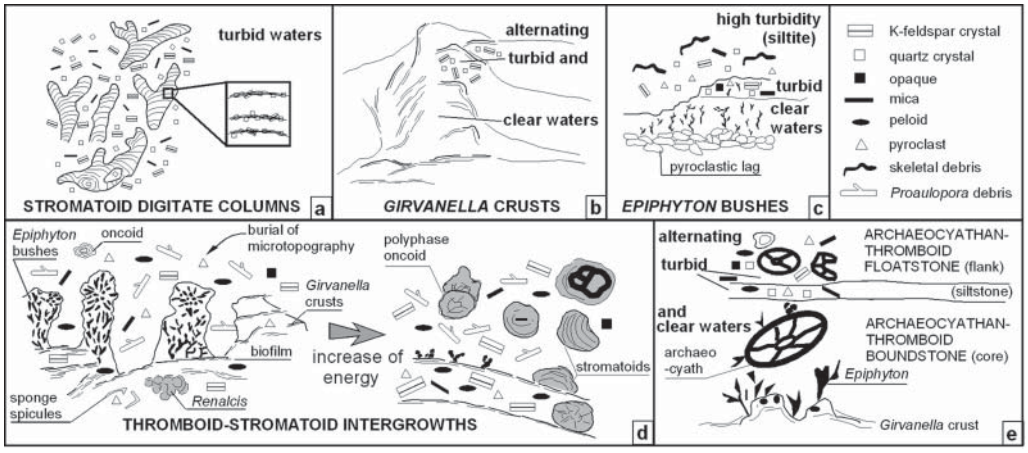

Fig. 8. Main types of microbial reefs in the Lemdad Formation of the Lemdad syncline.

fault-bounded crustal blocks. Synsedimentary deformation at the onset of reef sedimentation suggests that local topography/bathymetry was controlled by displacements on nearby faults.

The Botoman microbial reefs of the High Atlas platform grew under turbid waters associated with low–medium pyroclastic input. Reefs and crusts nucleated on protected (back-shoal) substrates and on low-relief bathymetric highs associated with migrating carbonate grainstone shoals and tectonic highs. The pioneer stabilization phase, which represents the sole of numerous reefs, was made by encrusting microbial biofilms and mats (e.g. *Girvanella* crusts). Tectonic instability and pyroclastic blanketing changed this environmental mosaic, favouring development of archaeocyathan–microbial reef complexes. These appear to have formed episodically on isolated topographic highs protected from pyroclastic input, grew under clear waters, and their demise coincided with flooding and shale onlapping. Bathymetry alone did not control where the reef complexes formed, as most of the potentially contemporaneous platform lithofacies were deposited within the same depth range. Probably more important were local hydrodynamic conditions determined in part by surrounding structurally controlled submarine topography. Formation of such reef complexes may have been favoured when peculiarities of local submarine topography damped or blocked effects of prevailing wind-generated waves and tidal currents.

Loose pyroclastic material frequently reworked and redeposited by marine processes. It mixed with shoal (grainstone barrier) and back-shoal (protected) microbial reef cores, and archaeocyathan–microbial flanks, whereas archeocyathan–microbial cores developed under low pyroclastic input (Fig. 8). Some microbial communities tolerated a continuous or episodic pyroclastic influx, approximately equal to their production rates. Reduced water clarity resulting from turbidity, associated with pyroclastic input, is interpreted as a key control on local nucleation of reefs. Nutrient input, often associated with increased land-derived epiclastic input, was not a primary factor as the terrigenous input in the southern High Atlas was dominantly pyroclastic. The thromboid and stromatoid microbial crusts and reefs developed under turbid waters are not very different from better-studied clear-water counterparts from the Moroccan Anti-Atlas or the Montagne Noire (Monninger 1979; Schmitt 1979; Álvaro *et al*. 1998, 2006). Patterns that enabled these microbial organisms to inhabit areas affected by pyroclastic input may have included changes into heterotrophic feeding. Morphological changes among photoautotrophic mats and biofilms to maximize the surface area available to incident light (Wilson 2000; Wilson & Lockier 2002) are not recognized in the microbial reefs of the High Atlas.

On a larger scale, the progressive demise of carbonate factories across Botoman times (Lemdad and Issafen formations) was sharply affected by the onset of the global Hawke Bay Regression. This is represented in the High Atlas and Anti-Atlas platforms by the prograding Asrir and laterally equivalent formations (Álvaro *et al*. 2003), which mark the disappearance of both microbial and archaeocyathan–microbial reefs.

Comparison of reef geometries: High Atlas v. Anti-Atlas platforms

The outcrops of the Lemdad syncline provide a key opportunity to compare the Botoman reef geometries and components between stable (Anti-Atlas) and unstable (High Atlas) platforms, where the effects of tectonic and volcanic activity directly controlled the development and subsequent demise of carbonate factories.

The Botoman interval marks the peak for Early Cambrian archaeocyathan–microbial reefs in West Gondwana (Álvaro *et al*. 2003). The dimensions achieved by these reefs in the Montagne Noire, southern France (Pardailhan and Lastours formations), Ossa-Morena, southern Iberian Peninsula (Sierra Gorda, La Hoya and Pedroche formations), central Iberian Peninsula (Navalucillos Formation), and Sardinia (Matoppa and Punta Manna formations) were largely exceeded by the Great Atlasian Reef Complex (GARC). The GARC was the largest reef complex of archaeocyathan–microbial reefs recorded on the western Gondwana margin. It extended, at least, for over 400 km along the Moroccan margin of West Gondwana, with a thickness peak in the Anti-Atlas platform. The GARC, in some cases more than 100 m thick, did not develop as an Australian-type Barrier Reef because the latter is separated from the shore by a wide lagoon, which is incompletely developed in the Anti-Atlas. Four geometries were distinguished by Álvaro *et al*. (2006) in the archaeocyathan–microbial reefs of the Botoman Amouslek Formation in the Anti-Atlas: (i) patches ranging in size from 0.2 to 2 m and from 0.2 to 1 m high, surrounded by well-bedded–massive shales; (ii) bioherms of greater dimensions (but less than 3.0 m thick), in which flank beds are well developed, and their margins commonly intercalate with lithologically variable interreef sediments; (iii) biostrome or low-relief structures (up to 1.2 m thick) comprising tabular or sheet-like beds, more than 10 m wide; and (iv) patch-reef complex, kalyptrae or kalyptrate complexes (*sensu* Rowland & Shapiro 2002), in which patches and bioherms occur stacked together (some of them more than 30 m thick) bounded by clay–marl–silt, millimetre- to centimetre-thick seams and discontinuities. Vertical kalyptrate complexes resulted by vertical accretion of numerous closely spaced bioherm and patch (grading laterally into biostromes) reefs.

During the same time span, contemporary rifting perturbations related to faulting and volcanic activity produced a distinct palaeotopography in the neighbouring High Atlas platform (Fig. 9). Faulting in the High Atlas platform caused localized tilting, subsidence perturbations and sedimentation of slope-related facies. The episodic volcanic activity became the source of vast quantities of pyroclastic material, which induced the spread of turbid waters and limited the northwards development of the GARC carbonate factories, dominantly composed of clear-water archaeocyathan–microbial reefs. Despite this, scattered reef complexes nucleated on selective substrates throughout the southern High Atlas platform, but did not reach more than 3.5 m in thickness. The pyroclastic influx close to volcanic centres rapidly inhibited, and even buried, most of the few remaining areas of shallow-water carbonate productivity. Shelled and ooidal carbonate factories contemporaneous with episodic volcanism locally flourished incorporating pyroclastic material. Exclusively microbial carbonate factories relatively supported a moderate pyroclastic influx, as documented by their pyroclastic-rich textures.

Conclusions

This paper documents how an interplay of geodynamic factors controlled the carbonate productivity through time and space in the Botoman, carbonate–mixed High Atlas platform. The main factors that influenced the Botoman nucleation of carbonate productivity there were as follows.

- *Synsedimentary tectonism.* Normal faulting resulted in the formation of tilting, drowning of downfaulted blocks, and breccia sedimentation on adjacent footwall areas in the High Atlas platform. Subsidence in hanging-wall areas invariably caused irregular topographies and subsequent sharp erosion leading to incision of erosive discontinuities and deposition of lobe breccias in hanging-wall depocentres. Faulting drastically altered the morphology of the High Atlas platform and significantly reduced the available area for shallow-water nucleation of microbial and shelled carbonate factories.
- *Volcanism.* The mass influx of pyroclastic debris on the High Atlas platform rapidly smothered carbonate factories in many of the remaining habitable shallow-water areas of the High Atlas platform. Only in more distal areas of the basin (Anti-Atlas platform) and during episodes of low volcanic activity (High Atlas) was carbonate productivity renewed. When the rate of influx of pyroclastic debris

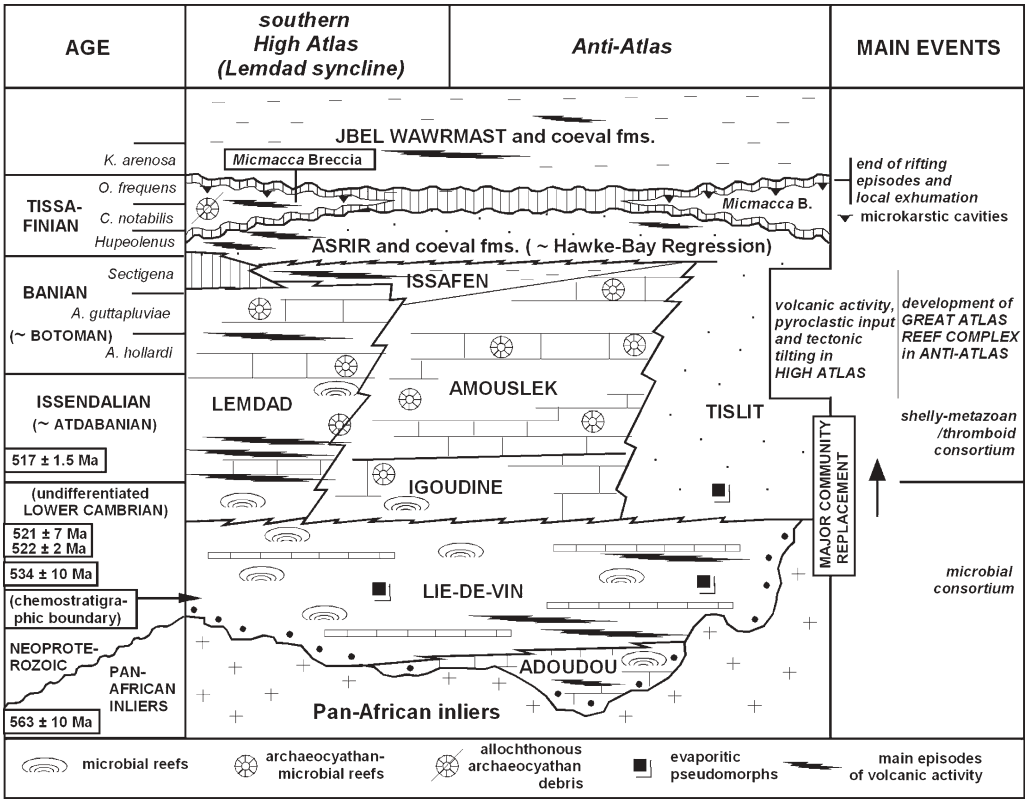

Fig. 9. Comparative stratigraphic framework of Lower Cambrian rocks from the southern High Atlas and Anti-Atlas; based on Leblanc & Lancelot (1980), Clauer *et al*. (1982), Latham & Riding (1990), Comptson *et al*. (1992), Debrenne & Debrenne (1995), Geyer & Landing (1995), Piqué *et al*. (1995), Landing *et al*. (1998), Álvaro *et al.* (2000, 2003, 2006), Gasquet *et al*. (2005), Álvaro & Clausen (2006) and this work.

was less than the accommodation rate of shallow-water carbonates, carbonate factories occurred coevally with volcanism. Then reefs nucleated on faulted highs, back-barrier (shoal) protected settings or directly over skeletal accumulations and pyroclastic substrates.

- *Relative sea-level fluctuations.* Numerous reported parasequences contain at their upper (shallower) part microbial reef patches and complexes. The end of their shallowing-upwards trends ended with either erosive contacts (filling by breccia and/or pyroclasts), probably related to syneruptive events, or sharp flooding and shale onlapping geometries, in both cases interrupting reef growth.

The scattered archaeocyathan–microbial reefs of the Lemdad Formation exhibit a wide range of external morphologies in the High Atlas platform, including tabular (biostromes) and domal (bioherms and patches) strata that vary considerably in size. Reef nucleation and growth were probably primarily controlled by local tectonism, as initial nucleation and accretion would have been facilitated by peculiar, hydrodynamic conditions imposed by irregular submarine topography perpetuated by faulting. Archaeocyathan–microbial reefs grew exclusively under clear waters, whereas microbial stromatoids, *Girvanella* crusts, *Epiphyton* bushes and thromboid–stromatoid intergrowths probably developed heterotrophic strategies when submitted to a moderate terrigenous input. Turbidity was a major ecological factor that constrained development of filter/suspension-feeder and phototrophic organisms, but not necessarily of benthic non-phototrophic microbial communities.

The authors thank F. Debrenne and O. Weidlich for their constructive reviews. This research was predominantly undertaken at the University of Lille I as part of an '*Innovative Thematic Action*' project entitled 'The

First Metazoan Reefal Communities Across the Neoproterozoic–Cambrian Transition in Morocco and South-western Europe'. This project also tried to improve the stratigraphic control on condensation and hiatus levels of chronostratigraphic stratotypes potentially candidates for future GSSP of the International Subcommission on Cambrian Stratigraphy and is a contribution to project CGL2006–13533.

References

Álvaro, J. J. & Clausen, S. 2005. Major geodynamic and sedimentary constraints on the chronostratigraphic correlation of the Lower–Middle Cambrian transition in the western Mediterranean region. *Geosciences Journal*, **9**, 145–160.

Álvaro, J. J. & Clausen, S. 2006. Microbial crusts as indicators of stratigraphic diastems in the Cambrian *Micmacca* Breccia, Moroccan Atlas. *Sedimentary Geology*, **185**, 255–265.

Álvaro, J. J., Vennin, E. & Vizcaïno, D. 1998. Depositional controls on Early Cambrian microbial carbonates from the Montagne Noire, southern France. *Transactions of the Royal Society of Edinburgh: Earth Sciences*, **89**, 135–143.

Álvaro, J. J., Rouchy, J. M. *et al*. 2000. Evaporitic constraints on the southward drifting of the western Gondwana margin during Early Cambrian times. *Palaeogeography, Palaeoclimatology, Palaeoecology*, **160**, 105–122.

Álvaro, J. J., Elicki, O., Geyer, G., Rushton, A. W. A. & Shergold, J. H. 2003. Palaeogeographical controls on the Cambrian trilobite immigration and evolutionary patterns reported in the western Gondwana margin. *Palaeogeography, Palaeoclimatology, Palaeoecology*, **195**, 5–35.

Álvaro, J. J., Clausen, S., El Albani, A. & Chellai, E. H. 2006. Facies distribution of the Lower-Cambrian cryptic microbial and epibenthic archaeocyathan-microbial communities in the western Anti-Atlas, Morocco. *Sedimentology*, **53**, 35–53.

Amorosi, A. 1995. Glaucony and sequence stratigraphy: a conceptual framework of distribution in siliciclastic sequences. *Journal of Sedimentary Research*, **B65**, 419–425.

Badra, L., Pouclet, A., Prost, A. E. & Touray, J. C. 1992. Mise en évidence d'une extension intra-plaque tardi-panafricaine d'intérêt métallogénique dans le Haut-Atlas occidental (Maroc). *Comptes Rendus de l'Académie des Sciences, Paris*, **314**, 703–709.

Boudda, A., Choubert, G. & Faure-Muret, A. 1975. *Coupe géologique de l'Ounein. Description lithologique*. Réunion sur la limite Précambrien–Cambrien, Agadir-Rabat, Documents, **A+B**.

Boudda, A., Choubert, G. & Faure-Muret, A. 1979. Essai de stratigraphie de la couverture sédimentaire de l'Anti-Atlas: Adoudounien, Cambrien inférieur. *Notes et Mémoires du Service Géologique du Maroc*, **271**, 1–96.

Chafetz, H. S. & Reid, A. 2000. Syndepositional shallow-water precipitation of glauconitic minerals. *Sedimentary Geology*, **136**, 29–42.

Choubert, G. 1958. L'Adoudounien et le Précambrien III dans l'Anti-Atlas. *Colloque International du CNRS, Paris (1957)*, **76**, 143–157.

Clauer, N., Caby, R., Jeanette, D. & Trompette, R. 1982. Geochronology of sedimentary and metasedimentary rocks of the West African Craton. *Precambrian Research*, **18**, 53–71.

Compston, W., Williams, J. L., Kirschvink, J. L., Zhang, Z. & Ma, G. 1992. Zircon U–Pb ages for the Early Cambrian time scale. *Journal of the Geological Society, London*, **127**, 319–332.

Debrenne, F. & Debrenne, M. 1995. Archaeocyaths of the Lower Cambrian of Morocco. *Beringeria*, **2**, Special Issue, 121–145.

Destombes, J., Hollard, H. & Willefert, S. 1985. Lower Palaeozoic rocks of Morocco. *In*: Hollard, C. H. (ed.) *Lower Palaeozoic Rocks of the World, Volume 4. Lower Palaeozoic of North-western and West Central Africa*. Wiley, Chichester, 157–184.

Ezzouhairi, H. 2001. *Le magmatisme post-collisionnel panafricain (tardi à post-orogénique) des régions d'Aghbalou, Sidi Flah Bouskour et Oued Imini (Ouarzazate, Anti Atlas central, Maroc). Lithostratigraphie, géochimie, pétrogenèse et contexte géodynamique*. PhD thesis, University of Chouaïb Doukkali.

Fisher, R. V. & Smith, G. A. 1991. Volcanism, tectonics and sedimentation. *In*: Fisher, R. V. & Smith, G. A. (eds) *Sedimentation in Volcanic Settings*. Society of Economic Paleontologists and Mineralogists, Special Publications, **45**, 1–5.

Gasquet, D., Levresse, G., Cheilletz, A., Azizi-Samir, H. R. & Mouttaqui, A. 2005. Contribution to a geodynamic reconstruction of the Anti-Atlas (Morocco) during Pan-African times with the emphasis on inversion tectonics and metallogenic activity at the Precambrian/Cambrian boundary. *Precambrian Research*, **140**, 157–182.

Geyer, G. 1990*a*. Proposal of formal lithostratigraphical units for the terminal Proterozoic to early Middle Cambrian of southern Morocco. *Newsletters on Stratigraphy*, **22**, 87–109.

Geyer, G. 1990*b*. Revised Lower to lower Middle Cambrian biostratigraphy of Morocco. *Newsletters on Stratigraphy*, **22**, 53–70.

Geyer, G. & Landing, E. (eds). 1995. Morocco '95. The Lower–Middle Cambrian standard of Gondwana. *Beringeria*, **2**, Special Issue, 1–171.

Heldmaier, W. 1997. *The Lower–Middle Cambrian transition along the northwestern margin of Gondwana (Anti-Atlas and High Atlas, Morocco)*. PhD thesis, Würzburg University.

Hupé, P. 1955. Iindices d'une phase tectonique salaïrienne dans l'Anti-Atlas marocain. *Comptes Rendus de l'Academie des Sciences de Paris*, **241**, 971–973.

Jouhari, A., El Archi, A., Aarab, M., El Attari, A., Emnih, N. & Laduron, D. 2001. Géochimie et cadre géodynamique du volcanisme néoprotérozoïque terminal (Vendien) du Haut Atlas occidental, Maroc. *Journal of African Earth Sciences*, **32**, 695–705.

KIDWELL, S. M. & BOSENCE, D. W. J. 1991. Taphonomy and time-averaging of marine shelly faunas. *In*: ALLISON, P. A. & BRIGGS, D. E. G. (eds) *Taphonomy: Releasing the Data Locked in the Fossil Record*. Topics in Geobiology. Plenum Press, New York, 115–209.

KRUMBEIN, W. E., BREHM, U., GERDES, G., GORBUSHINA, A. A., LEVIT, G. & PALINSKA, K. A. 2003. Biofilm, biodictyon, biomat microbialites, oolites, stromatolites geophysiology, global mechanism, parahistology. *In*: KRUMBEIN, W. E., PATERSON, D. M. & ZAVARIN, G. A. (eds) *Fossil and Recent Biofilms. A Natural History of Life on Earth*. Kluwer, Dordrecht, 1–28.

LANDING, E., BOWRING, S. A., DAVIDEK, K. L., WESTROP, S. R., GEYER, G. & HELDMAIER, W. 1998. Duration of the Early Cambrian: U–Pb ages of volcanic ashes from Avalon and Gondwana. *Canadian Journal of Earth Sciences*, **35**, 329–338.

LARCOMBE, P., COSTEN, A. & WOOLFE, K. J. 2001. The hydrodynamic and sedimentary setting of nearshore coral reefs, central Great Barrier Reef shelf, Australia: Paluma Shoals, a case study. *Sedimentology*, **48**, 811–835.

LATHAM, A. & RIDING, R. 1990. Fossil evidence of the location of the Precambrian/Cambrian boundary in Morocco. *Nature*, **344**, 752–754.

LEBLANC, M. & LANCELOT, J.R. 1980. Interprétation géodynamique du domain panafricain (Précambrien terminal) de l'Anti-Atlas (Maroc) à partir de données géologiques et géochronologiques. *Canadian Journal of Earth Sciences*, **17**, 142–155.

MEYER, R., KRAUSE, F. & BRAMAN, D. 1998. Unconformities within a progradational estuarine system: the upper Santonian Virgelle Member, Milk River Formation, Writing-on-stone Provincial Park, Alberta, Canada. *In*: ALEXANDER, C. R., DAVIS, R. A. & HENRY, V. J. (eds) *Tidalites: Processes and Products*. Society of Economic Paleontologists and Mineralogists, Special Publications, **61**, 129–142.

MYROW, P. 1998. Transgressive stratigraphy and depositional framework of Cambrian tidal dune deposits, Peerless Formation, central Colorado, USA. *In*: ALEXANDER, C. R., DAVIS, R. A. & HENRY, V. J. (eds) *Tidalites: Processes and Products*. Society of Economic Paleontologists and Mineralogists, Special Publications, **61**, 143–154.

MONNINGER, W. 1979. The section of Tiout (Precambrian/Cambrian boundary beds, Anti-Atlas, Morocco): an environmental model. *Arbeiten aus dem Paläontologie der Universität Würzburg*, **1**, 1–289.

ODIN, G. S. & FULLAGAR, P. D. 1988. Geological significance of the glaucony facies. *In*: ODIN, G. S. (ed.) *Green Marine Clay*. Elsevier, Amsterdam, 295–332.

OUAZZANI, H. 2001. Le volcanisme d'arc massif ancien du Haut Atlas occidental (Maroc), un témoin de la convergence de la branche occidentale de l'océan panafricain. *Bulletin de la Société géologique de France*, **172**, 587–829.

PIQUÉ, A., BOUABDELLI, M. & DARBOUX, J. R. 1995. Le rift cambrien du Maroc occidental. *Comptes Rendus de l'Académie des Sciences, Paris*, **320**, 1017–1024.

RIDING, R. 1991. Classification of microbial carbonates. *In*: RIDING, R. (ed.) *Calcareous Algae and Stromatolites*. Springer, Berlin, 21–51.

RIDING, R. 2002. Structure and composition of organic reefs and carbonate mud mounds: concepts and categories. *Earth-Sciences Review*, **58**, 163–231.

RIGGS, N. R., HURLBERT, J. C., SCHROEDER, T. J. & WARD, S. A. 1997. The interaction of volcanism and sedimentation in the proximal areas of a Mid-Tertiary volcanic dome field, central Arizona, USA. *Journal of Sedimentary Research*, **67**, 142–153.

ROWLAND, S. M. & SHAPIRO, R. S. 2002. Reef patterns and environmental influences in the Cambrian and earliest Ordovician. *In*: KIESSLING, W. & FLÜGEL, E. (eds) *Phanerozoic Reef Trends*. Society of Economic Paleontologists and Mineralogists, Special Publications, **72**, 95–128.

SCHMITT, M. 1979. The section of Tiout (Precambrian/Cambrian boundary beds, Anti-Atlas, Morocco): stromatolites and their biostratigraphy. *Arbeiten aus dem Paläontologie der Universität Würzburg*, **2**, 1–188.

SIEGERT, R. 1986. *Die klastischen Serien an der Wende von Unterzum Mittelkambrium im Anti-Atlas (Marokko)*. PhD thesis, Erlangen University.

SMITH, G. A. 1991. Facies sequences and geometries in continental volcanoclastic sequences. *In*: FISHER, R. V. & SMITH, G. A. (eds) *Sedimentation in Volcanic Settings*. Society of Economic Paleontologists and Mineralogists, Special Publications, **45**, 109–122.

SPIZHARSKI, T. N., ZHURAVLEVA, I. T., REPINA, L. N., ROZANOV, A. YU., TCHERNYSHEVA, N. YE. & ERGALIEV, G. H. 1986. The stage scale of the Cambrian System. *Geological Magazine*, **123**, 387–392.

VAN WAGONER, J. C., POSAMENTIER, H. W., MITCHUM, R. M., VAIL, P. R., SARG, J. F., LOUTIT, T. S. & HARDENBOL, J. 1988. An overview of the fundamentals of sequence stratigraphy and key definitions. *In*: WILGUS, C., HASTINGS, B., ROSS, C., POSAMENTIER, H., VAN WAGONER, J. & KENDALL, L. G. St. C. (eds) *Sea-level Changes – An Integrated Approach*. Society of Economic Paleontologists and Mineralogists, Special Publications, **42**, 39–45.

WILSON, M. E. J. 2000. Tectonic and volcanic influences on the development and diachronous termination of a Tertiary tropical carbonate platform. *Journal of Sedimentary Research*, **70**, 310–324.

WILSON, M. E. J. 2005. Development of equatorial delta-front patch reefs during the Neogene, Borneo. *Journal of Sedimentary Research*, **75**, 114–133.

WILSON, M. E. J. & LOCKIER, S. W. 2002. Siliciclastic and volcaniclastic influences on equatorial carbonates: insights from the Neogene of Indonesia. *Sedimentology*, **49**, 583–601.

WOOLFE, K. J. & LARCOMBE, P. 1999. Terrigenous sedimentation and coral reef growth: a conceptual framework. *Marine Geology*, **155**, 331–345.